TechPaper 6

TECHNICAL PAPER

An Experimentally Validated Dynamical Model of a Single-Track Hydrofoil Boat

G. P. van Marrewijk[1], J. K. Schonebaum[1], A.L. Schwab[2]

List of Symbols

Below, all symbols used in the paper are listed and named. Note that CoM stands for Center of Mass, while CoP stands for Center of pressure.

Capital Letters	Meaning	Unit
$\boldsymbol{A}$	State matrix	-
$\boldsymbol{B}$	Input matrix	-
$\boldsymbol{C}$	Output matrix	-
$C_{\mathcal{L}\alpha,s}$	Linear lift coefficient slope, struts	rad^{-1}
$C_{\mathcal{L}\alpha,w}$	Linear lift coefficient slope, wings	rad^{-1}
F	Force	N
I_{xx}	Mass moment of inertia about X-axis	$kg \cdot m^2$
I_{xz}	Mass moment of inertia about XZ-plane	$kg \cdot m^2$
I_{zz}	Mass moment of inertia about Z-axis	$kg \cdot m^2$
K	Inertia factor, see eqs. 16 to 18	$kg^{-1}m-2$
$\mathcal{L}_{nom,wf}$	Nominal lift force of front wing	N
$\mathcal{L}_{nom,wr}$	Nominal lift force of rear wing	N
L	Total hydrodynamic moment about X_b axis	$N \cdot m$
M	Total hydrodynamic moment about Y_b axis	$N \cdot m$
$\tilde{\boldsymbol{M}}_{cm}$	External moments about the center of mass	$N \cdot m$
N	Total hydrodynamic moment about Z_b axis	$N \cdot m$
S_{sf}	Submerged surface area of front strut	m^2
S_{sr}	Submerged surface area of rear strut	m^2
S_{wf}	Surface area of front wing	m^2
S_{wr}	Surface area of rear wing	m^2
V	Constant body velocity	m/s
X_b	X-axis of body reference frame	-
Y_b	Y-axis of body reference frame	-
Y	Total hydrodynamic force along Y_b	-
Z_b	Z-axis of body reference frame	-

Lowercase Letters	Meaning	Unit
b_{wf}	Front wing span	m
b_{wr}	Rear wing span	m
c	Wing chord	m
c_0	Root chord	m
c_{sf}	Front strut chord	m
c_{sr}	Rear strut chord	m
dx_{sf}	Front strut X_b-distance CoP to CoM	m
dx_{sr}	Rear strut X_b-distance CoP to CoM	m
dz_{fly}	CoM flight height above idealized waterline	m
dz_{id}	Offset between idealized and true waterline	m
dz_m	CoM flight height above true waterline	m
dz_s	CoM to end of strut	m
f	Frequency	Hz
g	Gravitational acceleration	m/s^2
ℓ	Local lift load per unit wing span	N/m
m	Total mass of boat and pilot	kg
p	Roll rate	rad/s
q	Pitch rate	rad/s
r	Yaw rate	rad/s
s	Semi-span of wing	m
t	Time	s
u	State-space input	rad
u	Velocity component in X_b direction	m/s
v	Velocity component in Y_b direction	m/s
w	Velocity component in Z_b direction	m/s
x	State vector of boat	Multiple
y	Coordinate along wing-span axis	m

Greek Letters	Meaning	Unit
γ	Steer angle	rad
δ_f	Front wing deflection	rad
δ_r	Rear wing deflection	rad
θ	Pitch angle	rad
ρ	Water density	kg/m^3
ϕ	Roll angle	rad
ψ	Yaw angle	rad
Ω	Rotation vector of the boat body	rad/s

---

[1] TU Delft Solar Boat Team, Stevinweg 4, Delft, The Netherlands
[2] Delft University of Technology, Biomechanical Engineering, Mekelweg 2, Delft, The Netherlands

Abstract

A single-track hydrofoil boat has two upside-down T-shaped hydrofoils that are placed behind each other on the centerline of the hull. To keep a single track hydrofoil boat upright during flight, the vertical front support strut is used as a rudder which the pilot steers into the direction of the fall. This is comparable to how a bicycle maintains lateral stability. A generalized dynamical model for single-track hydrofoil boats was developed to predict the roll and yaw motions under a steer input of the front strut. These motions were approximated analytically with conventional aircraft flight dynamics theory. The derivative coefficients that determine the coupling between state variables were derived from basic design parameters of the single-track hydrofoil boat. Validation of the model was done by experiments with the TU Delft Solar Boat 2016. The steer input, roll rate, yaw rate, roll angle, boat velocity and flight height were measured while the pilot generated a sinusoidal steer input at different frequencies and flight velocities. This data was compared with model predictions in the time and frequency domain. It was found that the model predictions are sufficiently accurate for model validation at steer input frequencies of 1 Hz and less. Therefore, the model can be used to design single-track hydrofoil boats and to simulate the dynamics in nominal flight conditions.

Introduction

The TU Delft Solar Boat Team competes every year in different championships for solar powered boats.[3,4,5] These boats are built to convert a limited amount of solar power into maximum forward race velocity. To reduce hydrodynamic drag, the team has been using hydrofoils since 2010.[6] In 2014 and 2016, the team based its solar boat concept on two fully submerged hydrofoils, each with an upside down T-shape and placed one behind another on the longitudinal axis of the boat. The front hydrofoil is used for steering. This concept is called a single-track hydrofoil boat and is comparable to single-track land vehicles such as the bicycle.

The single-track hydrofoil boat has several advantages: a fully submerged hydrofoil is more efficient than a surface piercing hydrofoil, because water surface effects are reduced.[1] Furthermore, the use of only two hydrofoils requires less supporting struts, which reduces mass and drag when compared to other hydrofoil concepts. This has resulted in a boat with a mass of 98 kg that is able to sail 30 km/h (16 knots) on solar power only and more than 50 km/h (27 knots) when battery power is also used. Typical maneuvers of take-off, straight flight and turning can be seen in Figure 3.


FIGURE 1. Kotaro Horiuchi has been designing and building single-track hydrofoil boats since the 1960's. Shown here is the OU32 single-track hydrofoil boat from 1988.[2]

Single track hydrofoil boats are not commonly used, although some notable examples exist, such as the Yamaha OU32 in Figure 1. It was developed by Kotaro Horiuchi, who designed and built single track hydrofoils at Yamaha. However, in his book,[2] he calls this type of boat a single strut hydrofoil, because when vie- wing the boat from straight ahead, one can only see a single strut.[2, p. 119] He states that besides being more efficient, single track hydrofoils can be more agile, more comfortable and more exciting to sail than multiple track hydrofoils.[2, ch. 4]

It is a challenge to make such a single-track hydrofoil boat laterally stable. Just like an inverted pendulum, it would tip over if no mechanism stabilizes it. The bicycle, an example of a single-track land vehicle, faces the same problem, but most bicycles can very well be ridden. The basic condition for stability is that the bicycle steers into the direction of the undesired fall.[3] When the dynamics of the single-track hydrofoil boat are sufficiently slow, this can be achieved by the pilot. To support the pilot in this task, gyroscope-based stabilization devices were proposed by Yokoyama and Horiuchi in a patent.[4]

---

[3] http://www.dutchsolarchallenge.nl
[4] http://www.nkzonnebootrace.nl
[5] http://www.yacht-club-monaco.mc/en/regattas-events/2016-uk/monaco-solar-boat-challenge
[6] http://www.solarboatteam.nl/en/history

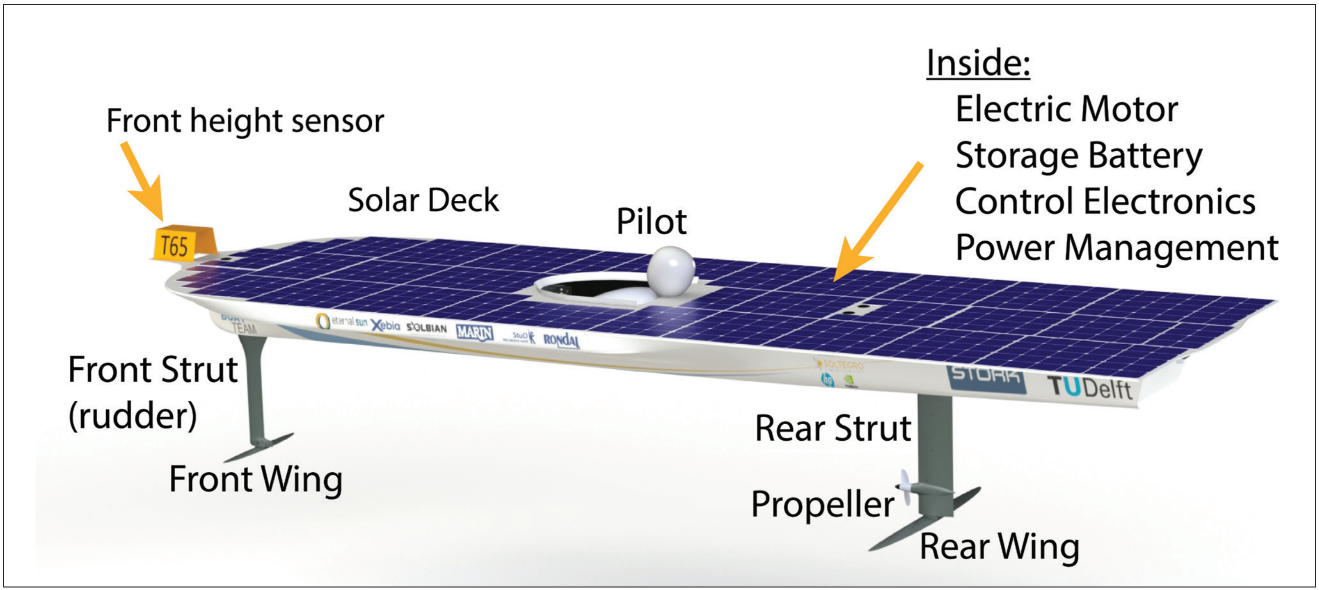

FIGURE 2. Design of the TU Delft Solar Boat 2016.


(a) Take-off

(b) Steady, straight and symmetric flight

(c) Turn to port side

(d) Turn to starboard side

FIGURE 3. Four typical maneuvers of a single-track hydrofoil boat: the TU Delft Solar Boat 2016.

Whether the single-track hydrofoil dynamics are sufficiently slow for control by a human pilot, depends on the boat flight dynamics. To predict the dynamics of a single-track hydrofoil boat design, a model has been developed. In this paper, we first present a novel model to simulate the dynamic behavior of pilot controlled single-track hydrofoil boats. Also, we describe how this model was validated by experiment.

This paper is structured as follows. After this introduction, the dynamical model is derived for the roll and yaw motions of single-track hydrofoils. Next, the experimental validation is described and results are shown. The paper ends with a discussion, conclusions and some recommendations for future research and applications of the model.

Single-track Hydrofoil Dynamics Model

The dynamical model was designed with the TU Delft Solar Boat 2016 in mind.[7] This single-track hydrofoil boat is shown in Figure 2 and typical maneuvers are displayed in Figure 3. The front and rear hydrofoil consist of a vertical strut and a horizontal wing. Both the struts and wings are considered as stiff aluminum structures.

Model parameters

As will be shown in this section, the only model parameters that are required those shown in Table 2. This table lists the parameter values and units for the TU Delft Solar Boat 2016. They are visualized in Figure 5. Note that it is assumed that the linear lift coefficient slopes are equal on both struts and on both wings. So, there is no distinction between $C_{\mathcal{L}\alpha,w}$ for both wings and for $C_{\mathcal{L}\alpha,s}$ for both struts.

Surface effects, such as described in [1], cause a lower lift force than expected for wings and struts near the water surface. In practice, this means that the top few centimeters of the struts generate waves and water spray, reducing the energy available for the generation of a lift force.[5, p. 197] This effect virtually increases the flight height. In the model, this is taken into account by taking the flight hight with respect to an idealized waterline that is a distance dz_{id} below the actual waterline. So, with a measured flight height dz_m, we obtain:

$$dz_{fly} = dz_m + dz_{id} \tag{1}$$

Currently, a fixed offset of 0.2 m in flight height is used, since this is slightly more than one rear strut chord length.[1] This leads to a typical idealized flight height of $dz_{fly} = 0.7$ m. In the Results, Section 4, the sensitivity of this setting is addressed.

Input	Symbol	Value (Average)	Unit
Water density	ρ	1000	kg/m^3
Gravitational acceleration	g	9.81	m/s^2
Constant body velocity	V	10	m/s
Total mass of boat and pilot	m	167	kg
Linear lift coefficient slope, wings	$C_{\mathcal{L}\alpha,w}$	5.7	rad^{-1}
Linear lift coefficient slope, struts	$C_{\mathcal{L}\alpha,s}$	6.67	rad^{-1}
Front strut chord	c_{sf}	0.089	m
Rear strut chord	c_{sr}	0.177	m
CoM to effective end of strut	dz_s	0.9	m
CoM flight height above true waterline	dz_m	0.5	m
Offset between idealized and true waterline	dz_{id}	0.2	m
Surface area of front wing	S_{wf}	0.0319	m^2
Surface area of rear wing	S_{wr}	0.0681	m^2
Front strut X_b-distance CoP to CoM	dx_{sf}	2.53	m
Rear strut X_b-distance CoP to CoM	dx_{sr}	1.38	m
Front wing span	b_{wf}	0.708	m
Rear wing span	b_{wr}	0.997	m
Mass moment of inertia about X-axis	I_{xx}	18.3	$kg \cdot m^2$
Mass moment of inertia about Z-axis	I_{zz}	219.1	$kg \cdot m^2$
Mass moment of inertia about XZ-plane	I_{xz}	-2.9	$kg \cdot m^2$

TABLE 2. Model parameters and values for the TU Delft Solar Boat 2016. Note that CoM stands for Center of Mass and CoP for Center of Pressure.

The submerged strut areas can be found from the chord length and flight height. Since the submerged struts have no taper:

$$S_{sf} = c_{sf}\,(dz_s - dz_{fly}) \tag{2}$$

$$S_{sr} = c_{sr}\,(dz_s - dz_{fly}) \tag{3}$$

All variables used throughout this paper can also be found in the List of Symbols, see page 135*.

Derivation of a Dynamical Model for the TU Delft Solar Boat

To find the generalized dynamic behavior of the single-track hydrofoil boat, a simplified model of the boat dynamics was developed. The TU Delft Solar Boat 2016 was modeled as a system of four rigid bodies, interconnected by idealized joints, as shown in Figure 4. The

---

[7] From here on, with "the boat" we refer to the TU Delft Solar Boat 2016

*Page number is pink because it's subject to change model conventions are based on those used in conventional aircraft flight dynamics.[6]

- The first or “primary” body consists of the boat hull, deck, internal parts, pilot and rear strut. It can rotate and translate freely in all three dimensions, resulting in a six degree of freedom (DoF) system. Since the pilot is part of this body, it is assumed that he or she does not move relative to other parts.
- The second body is the front strut. It is only able to rotate along its vertical axis. The angle of rotation of the strut chord with respect to the X_b-axis is the steer angle γ. See Figure 4.
- The third body is the front wing. It is fixed in position to the front strut. With respect to this strut, it can only rotate about the Y_b-axis. The front wing has its own actuator to set a control deflection δ_f along this Y_b-axis, which is used to actively control the flight height of the boat. See Figure 4 and Appendix A.
- The fourth body is the rear wing. It is fixed in position and in X_b-axis and Z_b-axis rotation, relative to the first body via the rear strut. A Y_b-axis control deflection δ_r can be performed by an actuator. It is controlled by the pilot as a sort of feed-forward control for the boat pitch angle, θ. To prevent the large solar deck from causing significant drag due to air resistance, the rear wing is set to a deflection angle which corresponds to near-zero boat pitch at the expected flight speed. See also Figure 4 and Appendix A.

From the above, we can conclude that the system has nine degrees of freedom: three primary body translations with velocity components $[u, v, w]$, three rotations with angular rates $[p, q, r]$ and three control deflections $[\gamma, \delta_f, \delta_r]$.

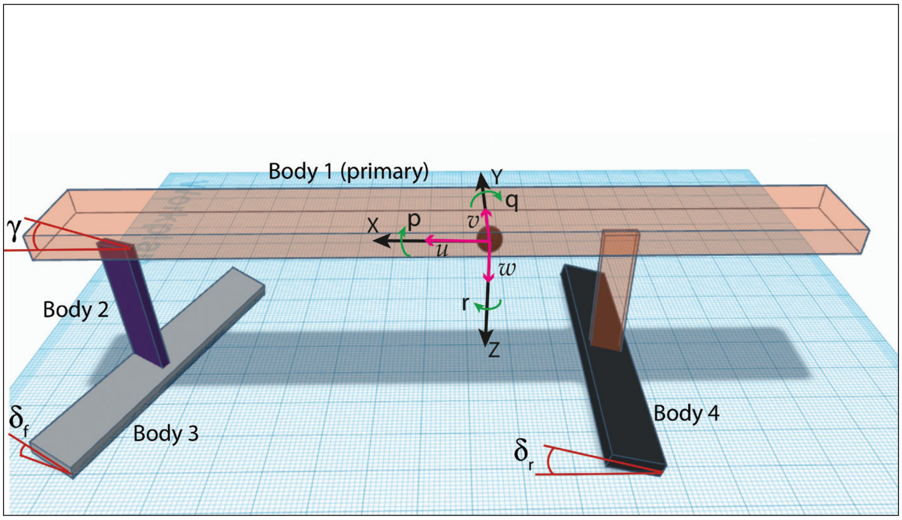

FIGURE 4: Illustration of the four body model. The first, primary body includes the hull, rear strut and pilot. The second body is the front strut with control input γ. The third body is the front wing, with deflection δ_f. Finally, body four has rear wing deflection δ_r. The body frame is located on the Center of Mass of the boat and aligned with the primary body. The boat velocity is given in the body frame by $[u,v,w]$ and the rotation rates by $[p,q,r]$.

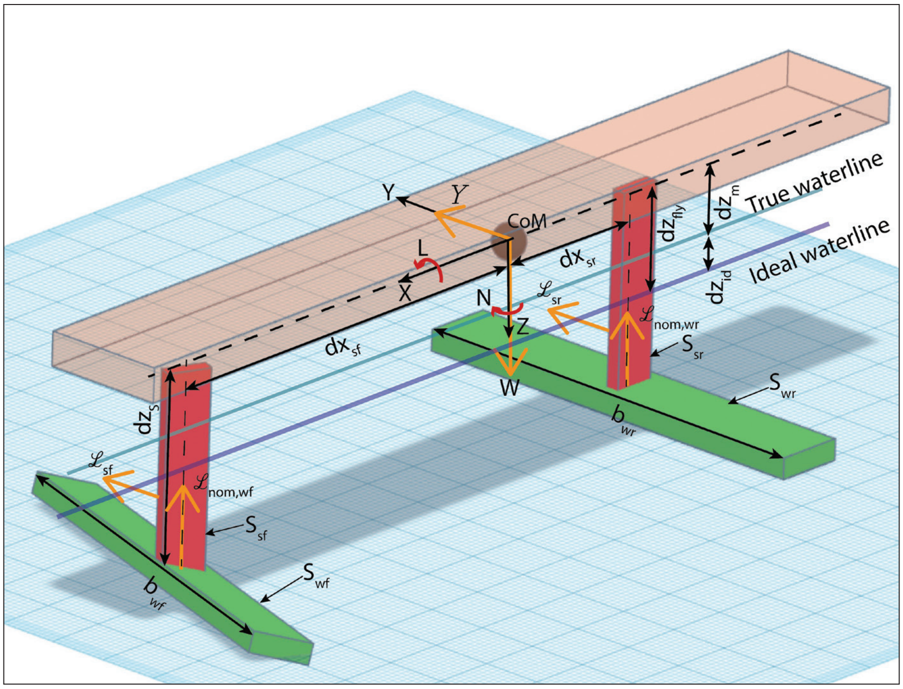

FIGURE 5: Dimensions and conventions used in the dynamical model of the hydrofoil boat. Body axes are indicated X, Y, Z. Weight vector $W = mg$ is located at the center of mass (CoM). Total hydrodynamic side force is given by Y. Relevant hydrodynamic moments are L about the X_b-axis and N about the Z_b-axis. Roll rate is indicated by p, yaw rate by r. Surface areas of the struts and wings are indicated by S. Parameters dx_{sf} and dx_{sr} denote the distance between CoM and the front/rear strut center of pressure, while $dz_{fly} = dz_m + dz_{id}$ gives the distance between CoM and idealized waterline. Strut length is denoted by dz_s. Front and rear wing have a span b_f and b_r, with a nominal lift of these wings indicated by $\mathcal{L}_f$ and $\mathcal{L}_r$. Steer input angle is given by γ. All variables are shown in positive direction.

The primary body orientation with respect to the inertial frame can be described as is done for aircraft, by the Euler angles of roll, pitch and yaw: $[\phi, \theta, \psi]$. For transformations between the inertial and body fixed reference frames, the order in which the Euler angles are applied is important, see Figure 16 in Appendix C. The body reference frame used in this paper is fixed and aligned to the primary body and has its origin at the center of mass of the boat, see Figures 4 and 5.

Translational motion

Newton's second law can be expressed in the body frame as:

$$m \left. \frac{d\boldsymbol{V}_{cm}}{dt} \right|_I^b = \boldsymbol{F}_{ext}^b \quad (4)$$

where:

- m is the mass of the boat.
- $\left.\frac{d\boldsymbol{V}_{cm}}{dt}\right|_I^b$ is the time rate of change of the boat velocity in the inertial frame, expressed in the body reference frame.
- $\boldsymbol{F}_{ext}^b$ are the total external force components on the body, expressed in the body reference frame.

They are given by the sum of the gravitational, hydrodynamic and aerodynamic forces in the body frame (denoted by subscript *dyn*):

$$\boldsymbol{F}_{ext}^b = mg \begin{bmatrix} -\sin\theta \\ \sin\phi\cos\theta \\ \cos\phi\cos\theta \end{bmatrix} + \begin{bmatrix} F_{x,dyn} \\ F_{y,dyn} \\ F_{z,dyn} \end{bmatrix} \quad (5)$$

The time rate of change of the velocity in the rotating body reference frame can be transformed to be expressed in body frame components:

$$\left. \frac{d\boldsymbol{V}_{cm}}{dt} \right|_I^b = \left. \frac{d\boldsymbol{V}_{cm}}{dt} \right|_b^b + \boldsymbol{\Omega}_{bI}^b \times \boldsymbol{V}_{cm}^b \quad (6)$$

where:

- $\left.\frac{d\boldsymbol{V}_{cm}}{dt}\right|_b^b$ is the time rate of change of the boat velocity in the body frame, expressed in the body frame.
- $\Omega_{bI}^b = [p, q, r]^T$ are the rotation vector components in the body fixed frame. See Figure 4.
- V_{cm}^b is the boat velocity, expressed in the body reference frame. In case there is no water current, we can write: $V_{cm}^b = [u, v, w]^T$. Combining Equations 4, 5 and 6 and expanding, we obtain the following equations that relate forces to accelerations:

$$m \begin{bmatrix} \dot{u} + qw - rv \\ \dot{v} + ru - pw \\ \dot{w} + pv - qu \end{bmatrix} = mg \begin{bmatrix} -\sin\theta \\ \sin\phi\cos\theta \\ \cos\phi\cos\theta \end{bmatrix} + \begin{bmatrix} F_{x,dyn} \\ F_{y,dyn} \\ F_{z,dyn} \end{bmatrix} \quad (7)$$

Rotational motion

The angular acceleration of the boat is of interest for our analysis of the roll rate, pitch rate and yaw rate. Dynamical analysis of the Euler equation of motion yields:

$$\dot{\boldsymbol{\Omega}}_{bI}^b = \boldsymbol{I}^{-1} \left(\tilde{\boldsymbol{M}}_{cm}^b - \boldsymbol{\Omega}_{bI}^b \times \boldsymbol{I}\boldsymbol{\Omega}_{bI}^b \right) \quad (8)$$

where we have introduced:

- $\tilde{\boldsymbol{M}}_{cm}^b$, which denotes the external moments about the center of mass of the boat, expressed in body reference frame components: $(M_x, M_y, M_z)^T$.
- $\boldsymbol{I}$, the mass moment of inertia tensor:

$$\boldsymbol{I} = \begin{bmatrix} I_{xx}, -I_{xy}, -I_{xz} \\ -I_{xy}, I_{yy}, -I_{yz} \\ -I_{xz}, -I_{yz}, I_{zz} \end{bmatrix}$$

Kinematic attitude relations

The relations between the rate of change of the Euler angles (roll, pitch and yaw) and the body reference frame angular rates are given by the kinematic attitude equations:[6]

$$\dot{\phi} = p + q\sin\phi\tan\theta + r\cos\phi\tan\theta \quad (9)$$

$$\dot{\theta} = q\cos\phi - r\sin\phi \quad (10)$$

$$\dot{\psi} = q\frac{\sin\phi}{\cos\theta} + r\frac{\cos\phi}{\cos\theta} \quad (11)$$

Reduction of the Full Model for State Space Representation

To make the model suitable for state-space representation, the equations of motion and kinematic equations are linearized by applying a Taylor expansion and ignoring higher-order terms. Due to symmetry of the boat about the XZ-plane, the first order hydrodynamic effects cancel each other: a change in the orientation and motion of the body XZ-plane does not affect the XY- and YZ- planes and vice versa.[6, p. 110] So, as is common in conventional aircraft flight dynamics, the resulting equations can be split into *symmetric* and *asymmetric* equations of motion.[6, 7] The symmetric equations describe the dynamics in the XZ-plane, whereas the asymmetric equations describe the dynamics in the XY and YZ-planes. We focus on asymmetric motions here, which are related to sway, roll and yaw motions of the boat. This implies that we do not focus on pitch, heave and surge. However, a qualitative description of the pitch and height control on the system of the boat is given in appendix A for completeness.

The steer angle γ is the control variable of the system, and is considered as input. This means that the state of the boat is defined by sideslip v, roll angle ϕ, roll rate p and yaw rate r.

Assumptions

The following assumptions were made to reduce the model to a simpler form:

- There are no external disturbances acting on the boat, such as waves, wind or currents. There are no forces other than the linearized hydrodynamic forces. Hence, $[u, v, w]^T$ is both the body velocity vector and the hydrodynamic velocity vector that determines the lift forces.
- The boat speed in X_b-direction is constant $u = const.$ and nonzero $u > 0$. This implies that the forces from propeller thrust T and total drag D cancel out. Hence, $\dot{u} = 0$ and the total external force $F_{x,dyn} = 0$.
- We assume that the equations can be linearized about a point where there is no sideslip and sideforce $v_0 = 0$, $\dot{v}_0 = 0$, $Y = 0$ and $\dot{Y}_0 = 0$. The boat does not make a turn: $r_0 = 0$ and $\dot{r}_0 = 0$. There is no initial yaw angle, yaw rate, roll angle and roll rate: $\psi_0 = 0$, $\dot{\psi}_0 = 0$, $\phi_0 = 0$, $\dot{\phi}_0 = 0$, $p_0 = 0$ and $\dot{p}_0 = 0$.
- The height control system is perfect, so the pitch angle and derivative are always zero $\theta = 0$, $\dot{\theta} = 0$, $q = 0$ and $\dot{q} = 0$. This implies that the sum of moments about the Y-axis is zero: $M = 0$. Also, Z_b-axis velocity and its derivative are always zero, because the vertical forces add to zero: $F_z = 0$, $\dot{F}_z = 0$, $w = 0$ and $\dot{w} = 0$. Hence, the symmetric equations of motion can be ignored. This also implies that the front and rear wing control angles δ_f and δ_r are not relevant for this simulation. This is a safe assumption, since in case of the TU Delft Solar Boat, the pitch angle and height above the waterline are kept constant by a control system that is independent of the roll and yaw motions. Furthermore, from real flight data, the flight height variation is found to be small. See Figure 6 in Section 4.
- The wings and struts are independently operating lifting surfaces that do not interfere with each other's velocity fields or the water surface. This assumption greatly simplifies the model, but is only partly valid: in reality there will be an influence,[1, 8] but it is expected to be small due to the relatively large distance between the hydrofoils. For roll angles above ca 30°, the wing tip can encounter surface effects. This would reduce the roll moment.[1] These roll angles will not be reached.
- All lift inducing surfaces operate in the range where lift is assumed to be linear with the angle of attack, α. This linearity assumption is valid for two-dimensional airfoil shapes and small angles on three-dimensional wings.[8, p. 344] Also, $C_{\mathcal{L}\alpha,w}$ is assumed equal for both wings, and $C_{\mathcal{L}\alpha,s}$ is assumed equal for both struts.
- Three-dimensional flow effects are ignored and the lift coefficient is assumed constant over the entire wing. The wings have no sweep angle and no dihedral angle. They are of perfect elliptical planform shape, based on a single airfoil design along the span. The high aspect ratio and elliptical shape of the wings ensure that induced vortices at the wing tips are small.[8, p. 430] The Solar Boat 2016 hydrofoils were designed with elliptical planforms, without sweep or dihedral, making this a safe assumption.
- The Z-axis steering rotation of the front wing on the front strut is ignored. So, steering angle γ does only affect front strut lift. This assumption implies that steering with the front strut does not rotate the front wing with it, even though they are coupled in reality. Y_b-direction lift forces caused by a steering angle on the front strut are estimated to be two orders of magnitude higher than changes in wing lift due to steering.
- Apart from the assumption that drag and thrust cancel out, other aerodynamic effects from all parts above the waterline are neglected. This can be assumed since water density is ca. 800 times higher than air density. Furthermore, the surfaces above the water are symmetric and were designed for zero lift and low drag. During testing, this assumption can be partly fulfilled if the tests are done with the boat sailing in downwind conditions at wind speed. Aerodynamic roll and yaw damping are still present in such a situation, but are considered negligible.
- The boat has a constant mass. Since no fuel is required for a solar boat, there is no change in mass during the tests.
- The mass distribution is symmetric with respect to the XZ-plane and constant in time. It is assumed that the pilot is positioned on the X-axis and does not move his/her mass. This enables us to ignore the inertia terms I_{xy} and I_{yz}. This assumption is valid when validation tests are performed with a pilot that does not move. For example, the pilot does not lean during cornering.
- Hydrodynamic constants do not change with velocity. This means that the lift coefficients, $C_{\mathcal{L}}$, are assumed to be independent of the Reynolds number.[8] It means that the dynamical model may not be accurate for velocities far from the reference velocity that was used to find the coefficients, which was ca. 10 m/s.
- Hydrofoil drag acts in the XZ-plane only. This means that only lift forces contribute to yaw and roll moments. In reality, a roll motion will cause a higher lift on one side of the hydrofoil, leading to a higher local drag. Compared to lift force, this drag effect is negligible.

With the above assumptions and linearization, we can rewrite the equations of motion and kinematic equations from Subsection 2.2. There are no disturbances, so the external forces and moments are only the hydrodynamic forces and moments. From here on, let $(L, M, N)^T$ denote the hydrodynamic moments about the X_b, Y_b and Z_b axes respectively. Let the hydrodynamic force in Y_b-direction $F_{y,dyn}$ be denoted by Y. Also, linearized derivatives are written with notation $y_x = \frac{dy}{dx}$. So for example, $N_p = \frac{dN}{dp}$ denotes the effect of a roll rate p on the Z_b-axis moment N. We obtain:

$$\begin{aligned} mg\phi + Y_v v + Y_{\dot{v}}\dot{v} + Y_p p + Y_r r + Y_\gamma \gamma &= m\left(\dot{v} + rV\right) \\ L_v v + L_p p + L_r r + L_\gamma \gamma &= I_{xx}\dot{p} - I_{xz}\dot{r} \\ N_v v + N_{\dot{v}}\dot{v} + N_p p + N_r r + N_\gamma \gamma &= I_{zz}\dot{r} - I_{xz}\dot{p} \\ \dot{\psi} &= r \\ \dot{\phi} &= p \end{aligned} \qquad (12)$$

State-Space Model of Asymmetric Motions

To describe the lateral boat dynamics, the asymmetric equations of motion from Eq. 12 were rewritten to a continuous linear time-invariant state-space model. The dynamics are described by:

$$\dot{\boldsymbol{x}}(t) = \boldsymbol{A}\boldsymbol{x}(t) + \boldsymbol{B}\boldsymbol{u}(t) \qquad (13)$$

$$\boldsymbol{y}(t) = \boldsymbol{C}\boldsymbol{x}(t) \qquad (14)$$

with $x(t)$ the state vector that describes the boat dynamics, A the state matrix that contains the state derivative coefficients, B the input matrix that relates the system input to the state change, C the output matrix (the identity matrix) and y the output vector. From Eq. 12, it can be seen that only four states are required to describe the motion and orientation of the boat. These are the velocity in Y_b-direction, roll angle, roll rate and yaw rate: $\boldsymbol{x}(t) = \left[v, \phi, p, r\right]^T$

Under our assumptions, the steering angle γ is the only system input. It is purely controlled by the human pilot. When a steering angle is applied, the front strut acts as a rudder and generates a lift pointing in the Y_b-axis direction. This lift has its center of pressure located on the rotation axis of the front strut, so no moment is generated that influences the steering angle. So we have:

$$\boldsymbol{u}(t) = \gamma(t) \qquad (15)$$

To make the state matrix easily readable, we define inertia factors K:

$$K_{xx} = \frac{I_{xx}}{I_{xx}I_{zz} - {I_{xz}}^2} \qquad (16)$$

$$K_{zz} = \frac{I_{zz}}{I_{xx}I_{zz} - {I_{xz}}^2} \qquad (17)$$

$$K_{xz} = \frac{I_{xz}}{I_{xx}I_{zz} - {I_{xz}}^2} \qquad (18)$$

From equation 12, the state matrix can be written as:[6]

$$\boldsymbol{A} = \begin{bmatrix} \frac{Y_v}{m} & \frac{Y_\phi}{m} & \frac{Y_p}{m} & \frac{Y_r}{m} - V \\ 0 & 0 & 1 & 0 \\ L_v K_{zz} + N_v K_{xz} & 0 & L_p K_{zz} + N_p K_{xz} & L_r K_{zz} + N_r K_{xz} \\ N_v K_{xx} + L_v K_{xz} & 0 & N_p K_{xx} + L_p K_{xz} & N_r K_{xx} + L_r K_{xz} \end{bmatrix} \qquad (19)$$

The input matrix $\boldsymbol{B}$ determines the effect of a steering angle γ on the state derivative $\dot{x}$. It is given by:

$$\boldsymbol{B} = \left[\frac{Y_\gamma}{m}, \quad 0, \quad L_\gamma K_{zz} + N_\gamma K_{xz}, \quad N_\gamma K_{xx} + L_\gamma K_{xz}\right]^T \qquad (20)$$

The linearized derivatives used in the matrices are derived in the next Subsection.

Linearized State Couplings

The derivative coefficients that describe the coupling between the states are required for the state and input matrices. They were approximated under the model assumption stated before. These approximations are based on the linearized lift change:

$$\Delta\mathcal{L} = \frac{1}{2}\rho V^2 S C_{\mathcal{L}_\alpha} \Delta\alpha \qquad (21)$$

For small changes in the angle of attack α, it can be approximated that $\sin\alpha = \alpha$ and $\cos\alpha = 1$. So, for an element in the X_bZ_b-plane (such as the struts) moving with a relative sideslip velocity v, or an element in the X_bY_b-plane with local Z-velocity w (such as the wings), the angles of attack change as:

$$\Delta\alpha = \frac{\Delta v}{V} \qquad (22)$$

$$\Delta\alpha = \frac{\Delta w}{V} \qquad (23)$$

Moment changes of the rigid body are calculated by multiplying the local lift change of an element with the distances to the principal axes. Next, with the stated assumptions and model parameters, the state derivative coefficients can be found.

Sideslip effects

A sideslip v causes an angle of attack on the front and rear strut, see eq. 22. Using eq. 21 with parameters from Table 2, it can readily be found that the struts generate a lifting force Y. Under linearization conditions, the Y-direction component of this force can be assumed to equal the total lift force and work opposite to v. Hence, the coefficient Y_v is negative. With S_{sf} and S_{sr} the submerged strut surface area, we get the total state derivative coefficient Y_v:

$$Y_v = -\frac{1}{2}\rho V C_{\mathcal{L}_\alpha,s}\left(S_{sf} + S_{sr}\right) \tag{24}$$

This sideforce causes a rolling and yawing moment, depending on distance of the CoP from the inertial axes:

$$L_v = \frac{1}{2}\rho V C_{\mathcal{L}_\alpha,s}\frac{dz_s + dz_{fly}}{2}\left(S_{sf} + S_{sr}\right) \tag{25}$$

$$N_v = \frac{1}{2}\rho V C_{\mathcal{L}_\alpha,s}\left(-S_{sf}dx_{sf} + S_{sr}dx_{sr}\right) \tag{26}$$

Roll angle effects

Under our assumptions, the only effect of a body roll angle ϕ is a tilt in the weight vector, when described in the body reference frame. The sideforce caused by the roll angle is approximated with the small angle approximation: $Y_{roll} = mg\phi$. So we have:

$$Y_\phi = mg \tag{27}$$

Roll rate effects

The roll rate p around the body X_b-axis changes the angles of attack on both struts and along the wing.

$\mathbf{Y_p}$

A positive roll rate causes a positive side force. Consider a small strut element, submerged at distance z from the CoM, with chord c_s and length dz. The angle of attack change is $\Delta\alpha = \frac{pz}{V}$. Inserting this in the lift equation gives:

$$\delta Y_{strut-element} = \frac{1}{2}\rho V^2 C_{\mathcal{L}_\alpha,s}\frac{pz}{V}c_s dz \tag{28}$$

The total side force generated due to a roll rate is found from integrating the above equation from distance dz_{fly} to dz_s:

$$Y_p = \frac{1}{2}\rho V C_{\mathcal{L}_\alpha,s}\left(c_{sf} + c_{sr}\right)\cdot\frac{1}{2}\left({dz_s}^2 - {dz_{fly}}^2\right) \tag{29}$$

Lp

The roll moment coefficient L_p originates from roll damping by the struts and hydrofoils. For the struts, we can write:

$$\delta L_{strut-element} = -\delta Y_{strut-element}\cdot z \tag{30}$$

For an element on the elliptical wing under a roll rate, the roll damping depends on the angle of attack: $\Delta\alpha = \frac{py}{V}$. Combining the integrand obtained from eq. 30 with the derivation from Appendix B.1, we obtain:

$$\begin{aligned} L_p = -\frac{1}{2}\rho V \Bigg(& C_{\mathcal{L}_\alpha,w}\cdot\frac{1}{16}\left(S_{wf}{b_{wf}}^2 + S_{wr}{b_{wr}}^2\right) \\ & + C_{\mathcal{L}_\alpha,s}\left(c_{sf} + c_{sr}\right)\cdot\frac{1}{3}\left({dz_s}^3 - {dz_{fly}}^3\right)\Bigg) \end{aligned} \tag{31}$$

Np

The generated side force from each strut in eq. 29 causes a Z_b-axis moment N . With a positive side force, the front strut causes a positive moment contribution and the rear strut a negative moment contribution. A roll motion also causes a tilt of the lift vector on the wings, which generates a negative contribution to N_p that depends on the nominal lift of the wing, $\mathcal{L}_{nom}$. See Appendix B.2 for a derivation. Combined, we get:

$$\begin{aligned} N_p = & \frac{1}{2}\rho V C_{\mathcal{L}_\alpha,s}\left(c_{sf}dx_{sf} - c_{sr}dx_{sr}\right)\cdot\frac{1}{2}\left({dz_s}^2 - {dz_{fly}}^2\right) \\ & -\frac{1}{16}\frac{1}{V}\left(\mathcal{L}_{nom,wf}{b_{wf}}^2 + \mathcal{L}_{nom,wr}{b_{wr}}^2\right) \end{aligned} \tag{32}$$

Yaw rate effects

The rigid body yaw rate causes an angle of attack change on the struts and an velocity along the wing spans. This results in a sideforce being generated by the struts and an asymmetric lift distribution on the wings. The resulting coefficients are given here.

Yr

The sideforce can easily be derived from the lift equation and angle of attack change:

$$Y_r = \frac{1}{2}\rho V C_{\mathcal{L}_\alpha,s}\left(-S_{sf}dx_{sf} + S_{sr}dx_{sr}\right) \tag{33}$$

Lr

The sideforce generated by the struts found above contributes to the body roll moment. Furthermore, the velocity difference along the wing span generates a rolling moment as described in Appendix B.3. Combined, we obtain:

$$\begin{aligned} L_r = {} & \frac{1}{2}\rho V C_{\mathcal{L}_\alpha,s}\frac{dz_s + dz_{fly}}{2}\left(S_{sf}dx_{sf} - S_{sr}dx_{sr}\right) \\ & + \frac{1}{8}\frac{1}{V}\left(\mathcal{L}_{nom,wf}{b_{wf}}^2 + \mathcal{L}_{nom,wr}{b_{wr}}^2\right) \end{aligned} \tag{34}$$

Nr

Under our assumptions, the wings do not contribute to a Z_b-axis moment under a yaw rate. The strut sideforces cause a damping moment:

$$N_r = -\frac{1}{2}\rho V C_{\mathcal{L}_\alpha,s}\left(S_{sf}{dx_{sf}}^2 + S_{sr}{dx_{sr}}^2\right) \tag{35}$$

Steer input effects

The pilot steering input γ has the effect of changing the angle of attack of the front strut, with $\Delta\alpha = \gamma$. From Figure 5, it can be seen that a positive steering angle causes a front strut lift in positive Y_b-direction. Hence, we write for the derivative of sideforce versus steering angle:

$$Y_\gamma = \frac{1}{2}\rho V^2 S_{sf} C_{\mathcal{L}_\alpha,s} \tag{36}$$

The corresponding roll moment is negative and depends on the CoP location of the submerged strut area:

$$L_\gamma = -\frac{1}{2}\rho V^2 S_{sf} C_{\mathcal{L}_\alpha,s}\frac{dz_s + dz_{fly}}{2} \tag{37}$$

Finally, the corresponding yaw moment is positive and depends on the strut distance from the CoM:

$$N_\gamma = \frac{1}{2}\rho V^2 S_{sf} dx_{sf} C_{\mathcal{L}_\alpha,s} \tag{38}$$

All coefficients for the linearized state space derivatives are now determined. When these are put into the equations 16 to 20, the state space model of the boat is complete and the dynamics can be analyzed.

Experimental Set-Up For Model Validation

To validate the state space model, tests were done with the TU Delft solar boat 2016 and data was gathered. This chapter explains what validation method was used and how the data was obtained.

Design of Model Validation Experiment

Bode Plot Comparison

As a Bode plot shows the dynamic behavior of a system in the frequency domain, it contains more information than a time-domain plot at one input frequency. Therefore, we have chosen to use Bode plots to validate our model. With the state space model, Bode plots of the system can be obtained. Such a plot is used to compare measured and calculated input/output relations of the boat. This can be done as follows: the pilot has to steer with a sinusoidal motion at a constant frequency (input). As a result, the boat will perform a roll, yaw and sideslip motion with the same frequency (outputs). The gain and phase shift between the steer motion and the output motions can be measured and drawn in a Bode plot. A measured signal always contains a spectrum of frequencies. Therefore, the steering was done such that the desired frequency was clearly the most prominent one in the signal. All other frequency content of the input signal is ignored. So, the slow corrections to keep the average roll angle zero can be ignored.

The shape of a Bode plot depends on all the system input variables (these are stated in Table 2). In Figures 9 - 11 the Bode plots of the roll angle (ϕ), the roll rate (p) and the yaw rate (r) are shown respectively as a line in the figures. They are plotted for four different velocities.

During tests, we measured the boat state variables under a given steer input frequency. The phase shift and magnitude of the experimental data at this frequency were plotted over the theoretical Bode plot lines. Only three out of four output states of the system have been evaluated, because the sideslip velocity (v) could not be measured with sufficient accuracy. This was due to the fact that only the total velocity of the boat was measured. It is hard to distinguish the contribution of the side slip component to the total velocity. Therefore, this state behavior is not presented in the results.

Variation of Velocity and Frequency Parameters

The design parameters shown in Table 2 were kept constant during testing, only the boat velocity (V) was varied between test runs. The boat flies stable at velocities greater than 7 m/s. The pilot was able to steer periodically up to 9.5 m/s. Therefore, tests were performed at 7.5, 8.0, 9.0 and 9.5 m/s respectively. Also the input frequency was varied at every test run. With some practical tests, we found that the pilot could steer with a maximum frequency of ca. 2 Hz. At low frequencies (less than 0.5 Hz) the pilot mainly corrects for the falling motion of the boat. A sine input at this frequency would create unsafe test conditions. Hence, the pilot was instructed to give a sinusoidal steer input of 0.5, 1.0 and 2 Hz respectively. These inputs had to be carried out for at least half a minute, to make at least five oscillations after settling of the dynamics. This results in twelve different test cases (i.e velocity - frequency combinations). Each test case was carried out at least twice.

The measured flight height was kept as constant as possible, varying between ca. 0.15 and 0.20 m, see also Figure 6 and Appendix A. Flying higher could have increased water surface effects on the wings, while a lower flight height would have caused the boat to hit wave crests. Both conditions would have violated the model assumptions. To verify that the flight height and velocity were constant during tests, these parameters were measured at all times and stored in a log file. Finally, the steer input was measured and logged, so as to check the exact steering frequency.

Test Environment

The tests were carried out on a canal that is 25 m wide and more than 3 m deep. During all tests, the maximum wind condition was a gentle breeze (Beaufort scale number 3) with varying direction. Since this canal is used by commercial freight ships, the water was disturbed a few times per hour. Therefore, some turbulence could not be avoided.

Experimental Setup for Data Collection

A sampling and saving frequency of 55 Hz for the input and output signals was used. All signals and their corresponding time stamps were stored on a data logger (Type Kvaser Memorator R SemiPro[9]) via the CAN bus (Controller Area Network) of the boat.

Measurement Equipment

Output and Velocity: The roll angle (ϕ), roll rate (p), yaw rate (r) and velocity (V) of the boat were measured using an Xsens Motion Tracker of type MTi-G-710.[10]This device measures position, velocity and accelerations in all translational and rotational directions. The typical accuracies of the measured roll angle, angular velocities and translational velocity are respectively 0.3°, 0.01°/s and 0.05 m/s. The Xsens Motion Tracker is located above the front strut, inside the hull.

Input: Steer input γ was measured with a hall effect steer sensor of type MHR5200 Magni- Hall.[11] The sensor is placed on the steering wheel. The angle of the steering wheel must be multiplied by a ratio of 0.26 to calculate the steer angle of the rudder. The hall sensor is an analog sensor, therefore a system in the boat converts the signal to an 8-bit digital signal. The conversion and ratio together result in an accuracy for the measurement of the steer input of 0.36°. For reasons explained in Section 2, it is assumed that no external moments are applied on the front strut and therefore steer system flexibility plays no role.

Height: The flight height of the boat was obtained using an ultrasonic water level sensor of the type Senix ToughSonic REMOTE 14[12] located just before the stem (front) of the boat. The influences of little waves on the water surface are of a higher order than the accuracy of this sensor. Therefore, we assume that the accuracy of this sensor does not influence our results.

Selection

The data of all test runs was evaluated with an algorithm that finds and isolates valid intervals of test data in the time domain. The algorithm searches for intervals that contain five periods of a target frequency. Next, it checks if the velocity and height of the boat are within target limits during the entire interval. The resulting intervals are checked manually to ensure no corrupted data was selected and that a clear sinusoidal input signal was measured. Finally, the gain and phase shift between the steer input and the state outputs are calculated. In this way, five successive oscillations in the time-domain data result in one point on the Bode plots.

Results

During the tests, the pilot experienced that steering with a frequency of 2 Hz was difficult. Therefore, he was instructed to try other frequencies between 1 Hz and 2 Hz. Using the defined selection criteria stated in Subsection 3.2, 179 time intervals were found. Typical interval flight height measurements are shown in Figure 6. As a result of the difficulty in steering at higher frequencies, much of the data of these tests was not usable. Therefore, only 48 of the 179 selected intervals have frequencies higher than 1 Hz. In this section, firstly two intervals will be shown in the time domain, subsequently all intervals will be presented in the frequency domain using Bode plots.

Time Domain

In the time domain, simulated responses can be plotted against measured states. Figures 7 and 8 show the dynamic behavior of the boat according to measurements and the model, for a measured steer input at two of the 179 time intervals. The model initial states had to be iteratively estimated up to ten decimal places to prevent the modeled boat from falling over to infinite roll angle. This effect was caused by the blind feeding of measured steer input to the model, without any form of feedback control.

It can be seen in Figure 7 that the model and measu- rements are almost identical, with only minor shifts in amplitude and phase of the response. Looking at e.g. the roll angle, the phase shift of the measurement is approximately 10° less than in the model predictions. The gain for both model and measurement are practically identical. It must be noted that the ideal water line parameter dz_{id} was kept at 0.20 m, as this resulted in the smallest error between theory and measurement.

Figure 8, on the other hand, shows a high difference between the measurements and the model. Particularly in the yaw rate, a smooth curve with higher maximums can be seen, whereas the measurement is very noisy and has peaks that are ca. 3° lower. Furthermore, an offset in phase can be seen for the roll rate. From the figure it can be estimated that the offset is about 36°. Note that the gain and phase differences were extracted from all 179 measurement intervals and subsequently plotted in the Bode plots.

Frequency Domain

Here we present the results in three Bode plots: one for the roll angle, roll rate and yaw rate respectively. In these figures we plotted the theoretical Bode plots generated by the model for four different speeds and average flight height. Furthermore, all 179 selected time intervals correspond to a point in the Bode plots. If multiple intervals were measured in a given frequency and velocity range, the mean value of the magnitudes and phase shifts of the signals was calculated. This mean value is drawn as a dot in the Bode plots. The size of a dot indicates the number of averaged measurements. The time domain measurements shown in Figures 7 and 8 were used to generate the red dots in the Bode plots (8 m/s) at 0.5 and 2.5 Hz respectively. From this, it can be seen that the 10° phase and almost zero gain offsets in Figure 7 is representative for the average offset at 0.5 Hz in Figure 9.

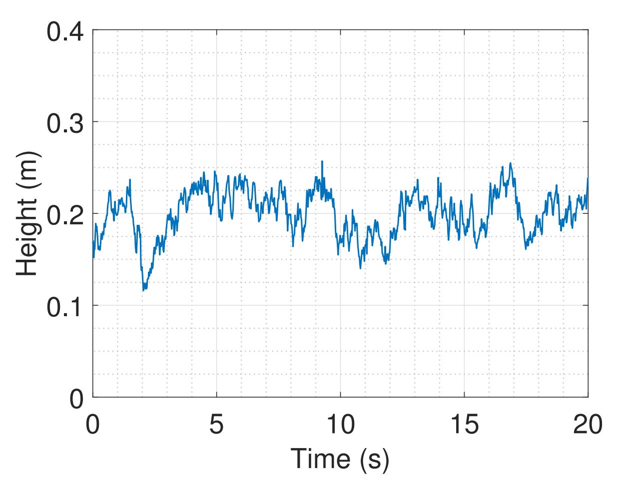

FIGURE 6. Typical output of the ultrasonic distance sensor during testing on canals. The high-frequency variation in height is caused by waves.

As for the time domain plots, the ideal water line parameter dz_{id} was kept at 0.20 m for maximum correlation between theory and results.

Analysis and Discussion of Results

In the previous section, we have seen the results. In this section, these results are analyzed and discussed. Both the phase and amplitude of the modeled and measured boat dynamics are very similar at frequencies below 1 Hz. This means that the predictions of the model are sufficiently accurate for practical use. However, in the frequency range of 1 Hz to 2.5 Hz, this similarity decreases and the results are less clear. The Bode plots show that the model most accurately predicts the dynamic behavior of the boat at 9.5 m/s and 0.5 Hz.

The predicted output gains increase with increasing velocity at all frequencies. This relation is confirmed by the measured data for all frequencies below 1.1 Hz. At higher frequencies, reliable and consistent measurements are scarce and hardly any conclusion can be drawn in this part of the spectrum. A very interesting feature in all Bode gain plots is found at 1.5 Hz. There, we observe a measured gain peak at all velocities, relative to the surrounding measurements. It looks as if a resonance occurs, but this is not predicted by the model.

In the Bode phase plots, it is predicted that there is a ca. 8° offset in phase with varying velocity. Note that roll rate

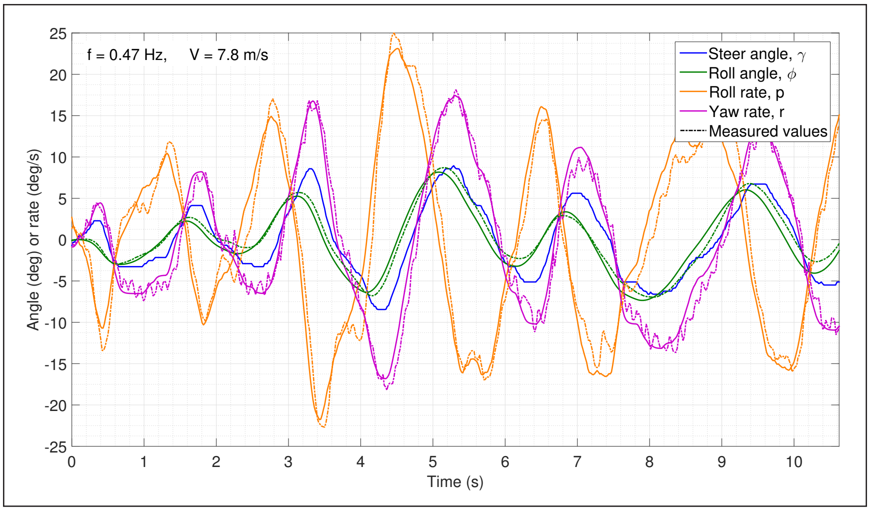

FIGURE 7. Modeled dynamics and measured dynamics in response to a given steer input γ for five periods of 0.47 Hz steer input. Continuous lines indicate model response, while dash-dot lines indicate the real measured response of the boat during testing. It can be seen that the model output is nearly identical to the measured output in both phase and amplitude. Velocity was 7.9 m/s and measured flight height ca. 0.15 m.

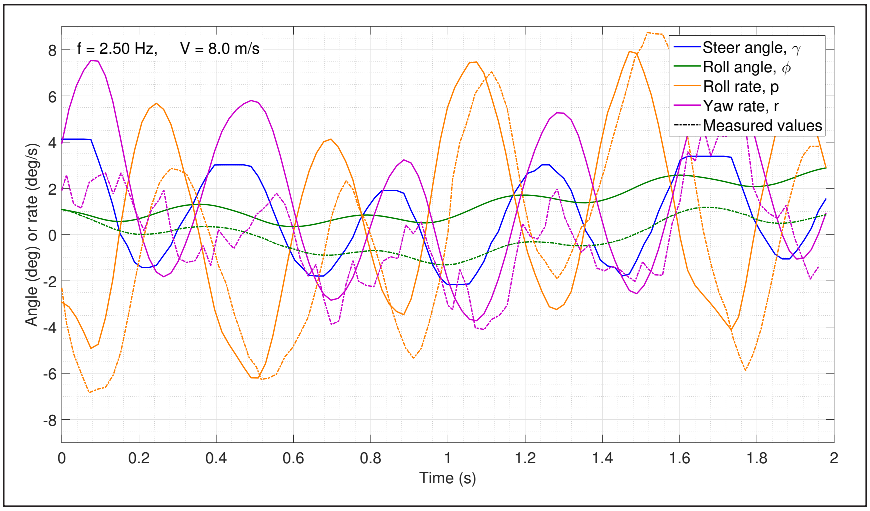

FIGURE 8. Modeled dynamics and measured dynamics in response to a given steer input γ for five periods of 2.50 Hz steer input. Continuous lines indicate model response, while dash-dot lines indicate the real measured response of the boat during testing. A small phase difference can be seen in the roll rate, while the yaw rate has an accurate phase prediction and erroneous amplitude prediction. Velocity was 8.0 m/s and measured flight height ca. 0.20 m. Note the scaling difference for the time and amplitude axes between this figure and Figure 7.

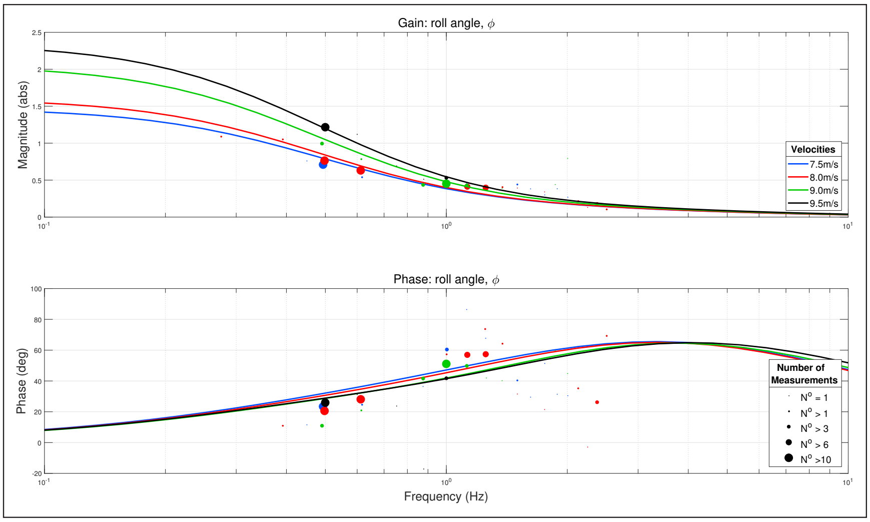

FIGURE 9. Bode plot that shows the frequency response of the input steer angle γ to output roll angle ϕ. The lines are the Bode plots calculated with the theoretical model. Every dot is the mean value of all measurements on a specific frequency. The size of the dots shows how many measurements it includes. Every dot resembles a time span of five periods of the signal. It can be seen that almost all measured points fall within a gain difference of 10% away from the model, especially at frequencies less than 1.3 Hz. Furthermore, we find that phase offset generally falls within 10 error margin. However, for frequencies above 1 Hz the difference increases and is more scattered. Figure 8 shows this as well.

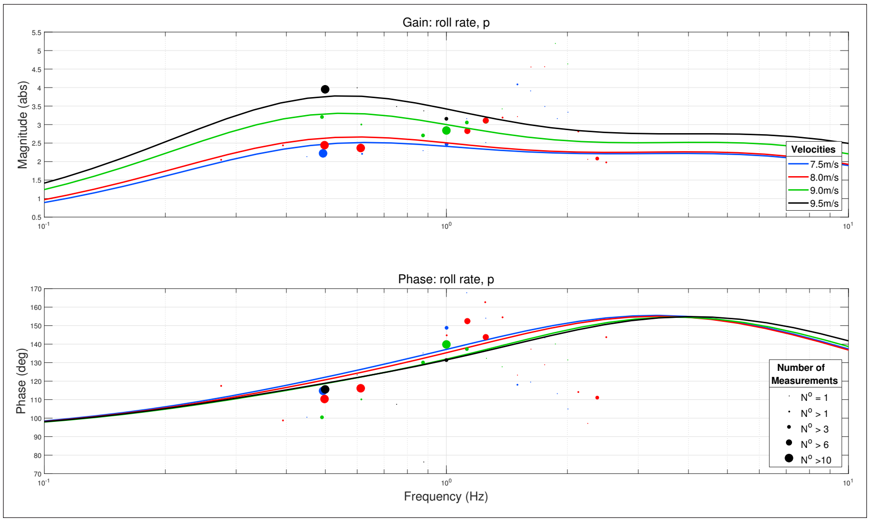

FIGURE 10. Bode plot that shows the frequency response of the input steer angle γ to output roll angle p. The lines are the Bode plots calculated with the theoretical model. Every dot is the mean value of all measurements on a specific frequency. The size of the dots shows how many measurements it includes. Every dot resembles a time span of five periods of the signal. We see that for 1 Hz and less, the gain difference is within 10% error margin. At ca. 1.5 Hz, however, we see that all measured gains are considerably greater than expected, but this peak is not seen anymore above 2 Hz. The measured phase shift, differs within 20 margin up to 1 Hz. At higher frequencies, this offset increases to a maximum error of more than 55 below expected values.

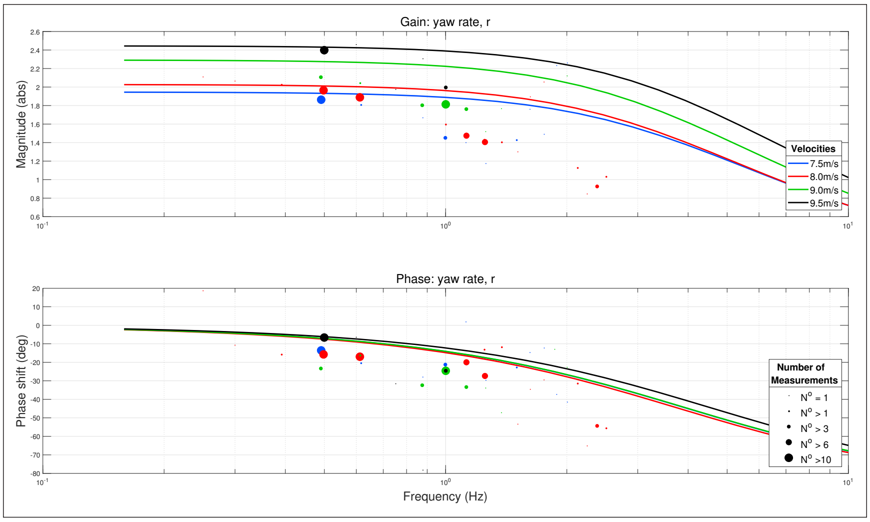

FIGURE 11. Bode plot that shows the frequency response of the input steer angle γ to output roll angle *r*. The lines are the Bode plots calculated with the theoretical model. Every dot is the mean value of all measurements on a specific frequency. The size of the dots shows how many measurements it includes. Every dot resembles a time span of five periods of the signal. The measured gain at 0.5 Hz shows little difference with the model. Above 0.5 Hz a clear downward trend can be noticed. This trend is predicted by the model, but at higher frequencies. The phase offset is no more than 20 below 1.3 Hz. Beyond this, it increases to a maximum error of 55.

and roll angle always have a phase difference of exactly 90°, both in theory and measurement. Figure 11 shows that the theoretical phase offset of the yaw rate is maximum for all states around 1.1 Hz. This cannot be confirmed by the measurements. Interestingly, the theoretical yaw rate phase plot for $V = 7.5$ and $V = 9.0$ m/s are identical, but the phase of $V = 8.0$ m/s is slightly lower. This cannot been confirmed with the data. As with the gain, the reliability of the measurements decreases with increasing input frequency.

The major frequency content of the steer input of the TU Delft Solar Boat 2016 normally lies below 1 Hz. Hence, the model predictions are useful and valuable for the TU Delft Solar Boat Team when normal operations are considered. Maneuvers with a high frequency content above 1 Hz can also be encountered, e.g. when the pilot has to recover rapidly from a sudden roll motion due to crosswind. For these sorts of situations, the model predictions can only be taken as a coarse reference.

During the derivation of the equations of motion in Section 2, some dynamical effects were ignored that may influence model accuracy. These are:

- Sensor noise was noticeable in the yaw rate and roll rate measurements, especially at high steer input frequencies when the input amplitude was below 5°, see Figure 8. The low signal-to-noise ratio may partly explain the large offsets in the Bode plot that can be seen in Section 4: noise increases the measured output signal and hence the relative gain. This effect can be reduced by filtering techniques.
- Flow over the rear hydrofoil is not only determined by boat motions, but also by the propeller flow field and induced wake of the front hydrofoil. Since the propeller of the boat is in front of the strut, as shown in Figure 2, a rotational flow field is generated. This violates the assumption of uniform, linear flow fields over the entire wings and struts and create unpredicted lift force changes.
- The pilot experiences that the boat “feels more sensitive to steer input when a cargo ship has just passed”. Cargo ships and variable wind caused disturbances in the water and the air. This may explain some of the differences between theory and experimental data points.
- The TU Delft Solar Boat 2016 has a finite stiffness, causing possible resonance modes that change the relative angles between the wings and struts. For example, torsional vibration motion of the hull along the boat Xb-axis can cause a difference in angle of attack at both struts. Also, torsional vibration along the rudder Z-axis might be induced by the steer actions of the pilot. This would cause different angles of attack along the front strut. Thus, under high frequency steer inputs, the infinite stiffness assumption may be violated.
- The assumption that all lifting surfaces operate with a constant and linear relation between lift coefficient $C_{\mathcal{L}}$ and angle of attack α may be violated at high steer input frequencies. For example, the more rapid the front strut is rotating about the steer axis, the lower the uniformity of the local velocity field. So, the assumption of a constant angle of attack does not hold.

Conclusions and Recommendations

This section explains the conclusions that are drawn from the experimental validation of the single-track hydrofoil boat model. Furthermore, recommendations are given on applications of the developed model and future research topics are suggested.

Conclusion

This paper presents a method from aircraft flight dynamics to establish a novel model for the dynamical behavior of a single-track hydrofoil boat. The boat was modeled as a system of four bodies interconnected by idealized joints. Only the asymmetric motions were considered. The model state is therefore fully determined by sideslip v, roll angle ϕ, roll rate p and yaw rate r. The only model input on the system is the pilot steering action, leading to a rudder steer angle γ.

The inverted T-shaped hydrofoils were modeled as four lifting surfaces that operate in the range where lift coefficient and angle of attack are linear. These four lifting surfaces are the front strut, rear strut, front wing and rear wing. The lift forces that are generated depend on the magnitude of the state variables and steer input. These influence the sum of forces and sum of moments about the center of mass of the boat. Under the assumption of small changes in angles of attack, the linearized state derivatives have been successfully calculated. With this, a linear time-invariant state space system has been created.

Flight tests have been performed under low-wind conditions. Different steer input frequencies and flight velocities were given to the boat and its roll angle, roll rate and yaw rate were recorded. Model predictions and actual flight test data have been compared in both the frequency domain and time domain. From this, it was found that the model almost exactly predicts the state of the boat for input frequencies of 1 Hz and lower. For frequencies above 1 Hz, the number of reliable measurement data is low and is scattered on the Bode plot. Nevertheless, the model can be used for accurately predicting the dynamics of single-track hydrofoils under typical flight conditions, i.e. low wind and water disturbances.

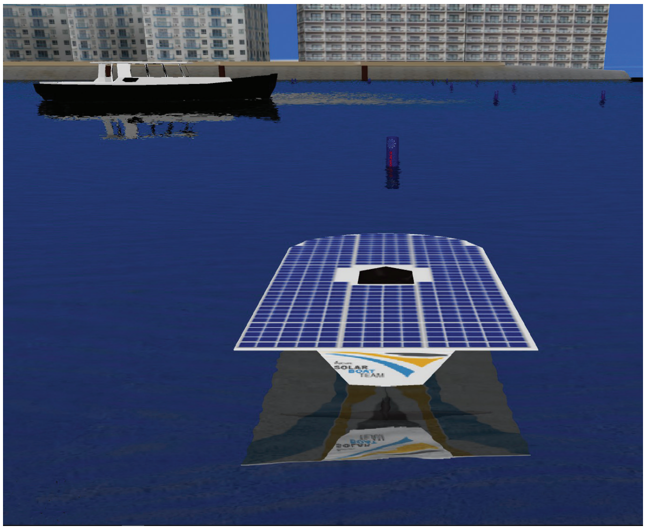

FIGURE 12. The dynamical model can be applied to simulators for pilot training, such as this Solar Boat Simulator PC-software that was developed by Thore Roepman from the TU Delft Solar Boat Team.

Therefore, it is concluded that the dynamical model of the TU Delft Solar Boat has been successfully validated by experiment up to steer inputs of 1 Hz. This means that future single-track hydrofoil boat designs can be simulated with this model before they are built, so that stability and agility can be evaluated.

Recommendations

An example of an application of the validated dynamical model is to use it in a real-time hydrofoil flight simulator, comparable with existing aircraft flight simulators. Teams such as the TU Delft Solar Boat Team could use these simulators to train pilots to fly the design before it will be built. See Figure 12 for a screenshot of one of the simulators. This simulator has recently been extended with the dynamical model, and is currently in the software test phase.

Besides this, the model can be used to predict the performance of a steer controller, should this be desired. Such a controller could be used to keep a single-track hydrofoil boat upright and on course. This would greatly reduce the control effort of the human pilot. It is expected that large single-track hydrofoil ships would need such a controller.[2, p. 139] The steer controller could be implemented in reality by electronic or mechanical means, see for example the patent of Yokoyama and Horiuchi.[4]

To improve model accuracy even more than what has been achieved, an optimization can be done on the boat parameters. For example, the boat mass moments of inertia are not exactly known. An optimization algorithm can be used to minimize the error between model output and measurement output.

Different topics for future research are recommended. Firstly, the reasoning and methods that were applied to the modeling and validation of the asymmetric dynamics can also be used to validate models for the symmetric dynamics. In this case, only two lifting surfaces and one inertia term will need to be taken into account, which should make such a model relatively easy to develop and validate. The derivations from Section 2 can be followed to obtain a state-space model, see also.[6, p. 112] Also, the same sensor setup can be used.

Secondly, research can be done to find higher order effects on the dynamics that were assumed negligible during this project. Some of these, such as the propeller flow or internal resonances of the structure, may have had an effect, see Section 5.

Acknowledgements

We would like to thank a few people. Firstly our adviser Arend Schwab. He came up with the idea for us to write this paper in the first place. He assisted us during the entire project, giving great feedback, pushing us in the right direction and giving us enough space to keep it our own project. Furthermore we would like to thank the following people for helping us in rain and sunshine to obtain the test data: Thore Roepman (pilot), Luc Does, Bart Vonk and Gijs Bruining. Also, our gratitude goes to the people who were so kind to review our paper and give their comments: Jodi Kooijman, Gerben Schonebaum, Casper Vertregt, Joost Willemse, Gijs Bruining and Hansje Schonebaum.

AUTHOR BIOGRAPHY

GIJSBERT VAN MARREWIJK is MSc. student in space systems engineering at Delft University of Technology, Faculty of Aerospace Engineering. Back in 2013, he worked full-time at the TU Delft Solar Boat Team as Chief Hydrofoil Dynamics and Stability, where he was responsible for the dynamics of the first solar-powered single-track hydrofoil boat ever. After cum laude completion of his BSc. in Aerospace Engineering, he advised the TU Delft Solar Boat Team during the development of their new single-track hydrofoil boat. When he does not write papers on hydrofoils, Gijsbert works on his MSc. thesis about deployable space telescope design.

JOHAN SCHONEBAUM is MSc. student in high tech engineering at Delft University of Techno- logy, Faculty of Mechanical Engineering (3mE). In 2013 he worked full-time at the TU Delft Solar Boat Team as hydrofoil engineer in the department of Dynamics and Stability. He was responsible for the structural design of the hydrofoils and the assembly and maintenance of the entire boat. Together with Gijsbert van Marrewijk and Jodi Kooijman he came up with the idea to use only two hydrofoils for the Solar Boat. Johan is editor of the reader for the BSc. course "Advanced Dynamics". He is an enthusiastic student, who likes to make music with his blues rock band.

REFERENCES

[1] S. F. Hoerner and H. V. Borst, "Fluid-dynamic lift: practical information on aerodynamic and hydrodynamic lift," *NASA STI/Recon Technical Report A*, vol. 76, p. 32167, 1975.

[2] K. Horiuchi and B. Michael, *Locus of a Boat Designer 2*. Cayuga Aqua Ventures, LLC, 2010.

[3] J. Kooijman, J. Meijaard, J. M. Papadopoulos, A. Ruina, and A. Schwab, "A bicycle can be self-stable without gyroscopic or caster effects," *Science*, vol. 332, no. 6027, pp. 339–342, 2011.

[4] F. Yokoyama and K. Horiuchi, "Lateral stabilization device for entirely submerged type hydrofoil craft," Nov. 27 1990, US Patent 4,972,792. [Online]. Available: https://www.google.nl/patents/US4972792

[5] A. F. Molland and S. R. Turnock, *Marine rudders and control surfaces: principles, data, design and applications*. Butterworth-Heinemann, 2011.

[6] B. Etkin and L. D. Reid, *Dynamics of Atmospheric Flight*. Wiley and Sons, Inc, 1996.

[7] W. J. Duncan, *The principles of the control and stability of aircraft*. Cambridge University Press, 1952.

[8] J. D. Anderson, *Fundamentals of Aerodynamics*, 5th ed. McGraw-Hill, 2011.

[9] KVASER@, *KVASER MEMORATOR R SEMIPRO*, KVASER@. [Online]. Available: www.kvaser.com

[10] Xsens, *MTi 100-series*, Xsens Technologies B.V. [Online]. Available: www.xsens.com

[11] MagniTec@, *Magni-Hall@ MHR5200 Series*, Magni-Tec @. [Online]. Available: www.magni-tec.com

[12] SENIX, *ToughSonic@ 14 Level and Distance Sensor*, Senix@ Corporation. [Online]. Available: www.senix.com

[13] R. Vellinga, *Hydrofoils: Design, Build, Fly*. Peacock Hill Pub., 2009.

[14] J. A. Mulder, W. H. J. J. van Staveren, J. C. van der Vaart, E. de Weerdt, C. C. de Visser, C. in 't Veld, and E. Mooij, *Flight Dynamics Lecture Notes*. Delft University of Technology, 2013.

Appendix

A. Digital Height Control

FIGURE 13. The Senix ToughSonic REMOTE 14[12] constantly measures the height of the boat.

To enable the boat to fly at a constant height above the water, a control system needs to be implemented that corrects the hydrofoil angle of attack. In this way, the wings always produce the right amount of lift. While most boats seem to use mechanical control systems to achieve this, the pitch and height control of the TU Delft Solar Boat 2016 are electronics based. This removes the need for a mechanical height sensor, which has significant drag. Also, it allows for digital tuning of the boat height and pitch, based on multiple sensor inputs. In the control loop, the sensors described in Section 3 are all used.

With these sensors, the full motion and orientation of the boat can be reconstructed. Typical height measurement output of the ultrasonic height sensor can be seen in Figure 6 in Section 3.

Five mbed™ development boards are used in the boat to collect data from the sensors and from the pilot input. The control error is defined as the difference between the measured height and the reference height. Because the ultrasonic sensor does measure distance between the boat and water in the Z_b, the roll angle is measured as well and used to correct the height measurement. The error function is further influenced by the boat pitch angle and pitch rate. Based on this error, a simple digital control loop on the mbed calculates the required wing angle update and sends this command to the actuator.

The actuator is a maxon motor with linear positioning spindle and encoder. It is located in the front side of the hull, directly above the front strut. The encoder keeps track of the motor position, while the linear spindle transfers the rotational motion to a linear motion. A carbon fiber rod in the front strut transfers this motion to the front wing. The effect is a change in control angle δ_f, as shown in Figure 14. This process is repeated at a rate of ca. 10 Hz, such that any disturbances in height are quickly compensated. To minimize the required control energy and improve take-off capability, a canard configuration was chosen.[13]

The control loop and data acquisition software on the control boards can be updated during tests, to find the optimum settings or "debug" the boat. See Figure 15. Also, the collected data and control system constants can be read and set by the crew remotely, using a laptop with mobile network communication. This enables the pilot to focus on operating the boat, while other crew members monitor performance. This is essential during long races, where changes in incoming solar power, wind, battery state, etc. require constant updates in the race strategy.

B. Derivative Coefficients

B.1 Roll damping of elliptical wing

The wings cause a damping of the roll moment. The roll damping of the wings is denoted by $L_{p,damp}$. We derive an analytical expression for this damping here.

Let s denote the semi-span of an elliptical wing surface based on a single airfoil design. Let c_0 denote the root chord of the hydrofoil. The wing is oriented with its span along the y-axis and travelling in x-direction. A roll motion causes a local change in lift along the span.

To find the roll damping moment induced by pure roll motion, L_{damp}, we can ignore the steady-state symmetric lift distribution along the wing span and only consider the moment caused by the local lift change $\delta\ell$:

$$L_{damp} = -\int_{-s}^{s} \delta\ell \cdot y \qquad \textbf{(39)}$$

where the minus sign indicates a damping effect. The local lift change is assumed to be linear with the change in local angle of attack. We use the lift equation for infinite segments along y-direction:

$$L_{damp} = -\int_{-s}^{s} \frac{1}{2}\rho V^2 \delta S(y) C_{\mathcal{L}_\alpha} \Delta\alpha(y) \cdot y \qquad \textbf{(40)}$$

The local change in angle of attack is the ratio between the rotation induced speed in vertical direction and the boat horizontal speed:

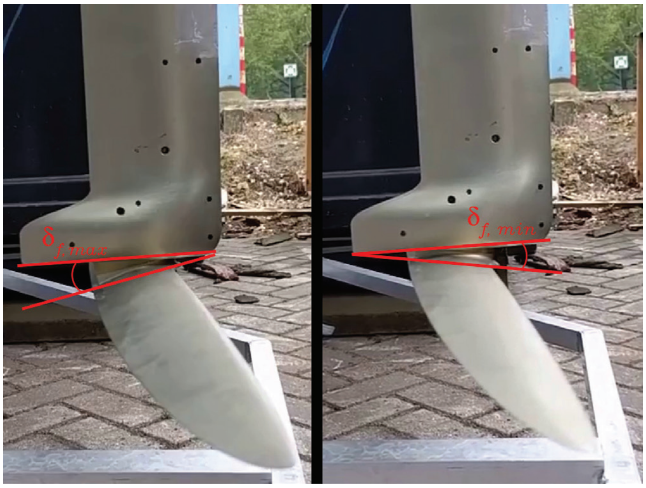

FIGURE 14. Maximum (left) and minimum (right) control deflection angle of the front wing (δ_f) .

$$\Delta\alpha(y) = \frac{py}{V} \tag{41}$$

The local surface area of an element is:

$$\delta S(y) = c(y)dy \tag{42}$$

with the local chord length $c(y)$ given by the equation for an ellipsoid:

$$c(y) = c_0\sqrt{1-\left(\frac{y}{s}\right)^2} \tag{43}$$

where s is the semi-span of the wing. Combining the above:

$$L_{damp} = -\frac{1}{2}\rho V c_0 C_{\mathcal{L}_\alpha} p \int_{-s}^{s} y^2\sqrt{1-\left(\frac{y}{s}\right)^2}dy \tag{44}$$

The integral term can be solved analytically and yields:

$$\int_{-s}^{s} y^2\sqrt{1-\left(\frac{y}{s}\right)^2}dy = \frac{\pi}{8}s^3 = \frac{\pi}{64}b^3 \tag{45}$$

where we have rewritten to incorporate the full wing span. Root chord c_0 can be written in terms of wing surface area and span using the equation for surface area of an ellipsoid:

$$c_0 = 2\frac{S}{\pi s} = \frac{4S}{\pi b} \tag{46}$$

Substitution of the above gives for the roll damping moment:

$$L_{damp} = -\frac{1}{2}\rho V S C_{\mathcal{L}_\alpha}\frac{b^2}{16}p \tag{47}$$

FIGURE 15. During tests, the crew is able to change the data-acquisition and height control software to find optimum settings. Data can be tracked live via a server and imported to software.

The derivative dL/dp or $L_{p,damp}$ is used in the state matrix:

$$L_{p,damp} = -\frac{1}{2}\rho V S C_{\mathcal{L}_\alpha}\frac{b^2}{16} \tag{48}$$

Note that the total coefficient L_p depends on roll damping of the two elliptical wings and the submerged parts of the two struts.

B.2 Roll-induced yaw of elliptical wing

In addition to the damping motion described above, the rolling motion of a wing causes a tilt in the local velocity vector of a wing element. E.g. when rolling to the right, the angle of attack of the right wing part increases and the local lift vector tilts forward, causing a negative yawing moment N . Assuming small angles, we get for the total yaw moment contribution of all wing elements:

$$N_{roll,wing} = -\int_{-s}^{s}\mathcal{L}(y)\cdot\Delta\alpha(y)y \tag{49}$$

The local lift coefficient is approximated by:

$$C_{\mathcal{L}}(y) = C_{\mathcal{L},nom} + C_{\mathcal{L}_\alpha}\Delta\alpha(y) \tag{50}$$

where $C_{\mathcal{L},nom}$ is the nominal lift coefficient in steady, symmetric flight. Substituting the general lift equation to eq. 49

$$N_{roll,wing} = -\int_{-s}^{s} \frac{1}{2}\rho V^2 c(y)dy \left(C_{\mathcal{L},nom} + C_{\mathcal{L}_\alpha}\Delta\alpha(y)\right) \cdot \Delta\alpha(y)y \quad \textbf{(51)}$$

Substituting eq. 41 and eq. 43:

$$N_{roll,wing} = -\frac{1}{2}\rho V^2 \frac{p}{V} c_0 \int_{-s}^{s} y^2 \sqrt{1-\left(\frac{y}{s}\right)^2} \left(C_{\mathcal{L},nom} + C_{\mathcal{L}_\alpha}\frac{py}{V}\right) dy \quad \textbf{(52)}$$

Splitting the integral:

$$N_{roll,wing} = -\frac{1}{2}\rho V^2 \frac{p}{V} c_0 C_{\mathcal{L},nom} \int_{-s}^{s} y^2 \sqrt{1-\left(\frac{y}{s}\right)^2} dy + C_{\mathcal{L}_\alpha}\frac{p}{V} \int_{-s}^{s} y^3 \sqrt{1-\left(\frac{y}{s}\right)^2} \quad \textbf{(53)}$$

The first integral is equal to eq. 45 and can be substituted by $\frac{\pi}{64}b^3$. The second integral term becomes zero due to symmetry. Eq. 46 can be substituted as well. We obtain:

$$N_{roll,wing} = -\frac{1}{2}\rho V S C_{\mathcal{L},nom} \frac{b^2}{16} p \quad \textbf{(54)}$$

which yields the state space coefficient N_p for one elliptical wing:

$$N_{p,wing} = -\frac{1}{2}\rho V S C_{\mathcal{L},nom} \frac{b^2}{16} \quad \textbf{(55)}$$

or equivalently:

$$N_{p,wing} = -\frac{\mathcal{L}_{nom}}{V}\frac{b^2}{16} \quad \textbf{(56)}$$

where $\mathcal{L},nom$ indicates nominal wing lift in steady, symmetric flight.

B.3 Yaw-induced roll of elliptical wing

In addition to the above state couplings, a yaw rate r will create a local x-velocity increase Δu over a wing element. The corresponding lift difference across the wing span causes a rolling moment $L_{yaw,wing}$. For one element with lift change $\delta\ell$, we follow eq. 39 and 40 to get:

$$L_{yaw,wing} = -\int_{-s}^{s} \delta\ell \cdot y \quad \textbf{(57)}$$

where the minus sign is required because a positive yaw rate will cause a negative $\delta\ell$ on a positive (right-wing) element dy, causing a positive rolling moment. Note that during a pure yaw motion, the angle of attack and lift coefficient are not expected to change. So we can write:

$$L_{yaw,wing} = -\int_{-s}^{s} \frac{1}{2}\rho\left(V + \Delta u(y)\right)^2 \delta S(y) C_{\mathcal{L},nom} \cdot y \quad \textbf{(58)}$$

The along-span speed change $\Delta u(y)$ is found by:

$$\Delta u(y) = -ry \quad \textbf{(59)}$$

since a positive yaw rate reduces the velocity on a positive wing element, the minus sign is required. For the TU Delft Solar Boat, the maximum Δu is in the order of 0.3 m/s, which is more than an order of magnitude below minimum take-off speed V_{min}. Therefore, we can linearise the quadratic term in eq. 58 and use $(V + \Delta u(y))^2 \neq V^2 + 2V\,\Delta u(y)$.

The integral term going with V^2 can be shown to be just the nominal wing lift in steady, symmetric flight. This causes no yawing moment. With the term $2V\,\Delta u(y)$, we obtain:

$$L_{yaw,wing} = -\frac{1}{2}\rho C_{\mathcal{L},nom} \cdot 2V \int_{-s}^{s} \Delta u(y)\delta S(y) \cdot y \quad \textbf{(60)}$$

Substituting eq. 42, 43 and 59 leads to:

$$L_{yaw,wing} = \frac{1}{2}\rho C_{\mathcal{L},nom} \cdot 2Vrc_0 \int_{-s}^{s} y^2 \sqrt{1-\left(\frac{y}{s}\right)^2} dy \quad \textbf{(61)}$$

With the substitutions from eq. 45, eq. 46 and $s = \frac{b}{2}$ we can simplify this to:

$$L_{yaw,wing} = \frac{1}{2}\rho V S C_{\mathcal{L},nom} \frac{b^2}{8} \cdot r \quad \textbf{(62)}$$

And we find the state derivative $L_{r,wing}$:

$$L_{r,wing} = \frac{1}{2}\rho V S C_{\mathcal{L},nom} \frac{b^2}{8} \quad \textbf{(63)}$$

his term shows that the wings will generate a positive rolling moment when the boat has a positive yaw rate.

C. Other figures

Below are some figures that were not considered essential in the main body text, but which may provide extra insight.

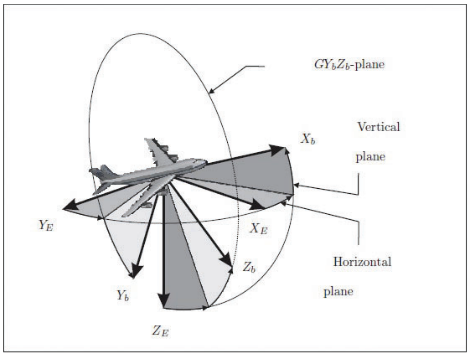

(a) Aircraft orientation

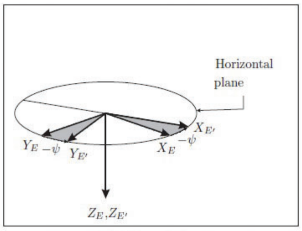

(b) 1st rotation: ψ

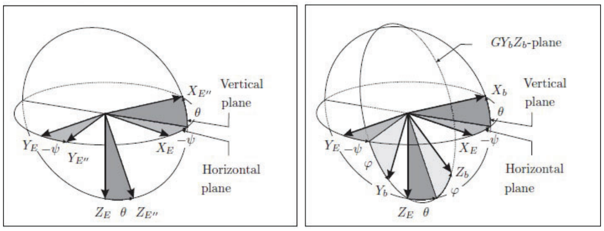

(c) 2nd rotation: θ (d) 3rd rotation: φ

FIGURE 16. The three-step transformation from the Earth reference frame to the body-fixed reference frame. The first of three consecutive rotations is a Z-axis rotation over the yaw angle. A negative yaw angle $-\psi$ was taken for illustrative purposes. Next, an Y-axis rotation over the pitch angle θ aligns the intermediate body frame with the aerodynamic reference frame. Finally, a rotation over roll angle ϕ is required. Obtained from [14].

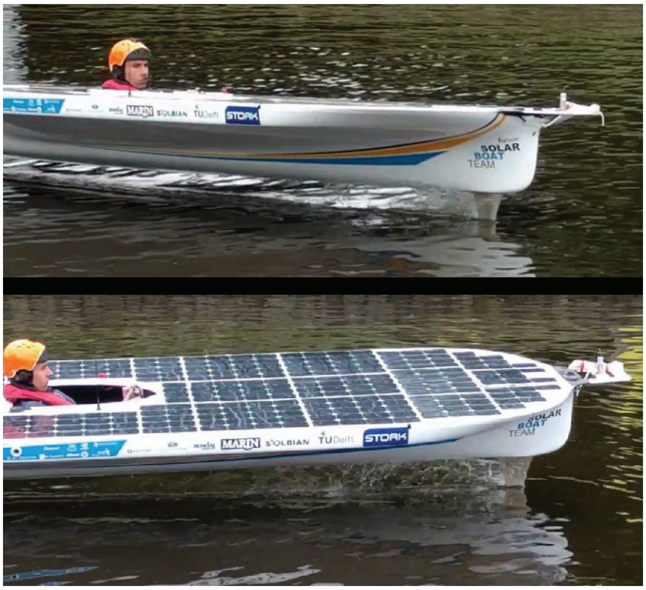

FIGURE 17. The sine-like input on the steer, given by the pilot, causes a rolling motion of the boat during data collection for dynamic model validation. Low-frequency steering input keeps the boat in upright position and is ignored in the data analysis.

FIGURE 18. The boat has successfully competed in the Dutch Solar Challenge 2016. Shown here is the neck-to-neck race against the triple wing hydrofoil from Clafis Victron Energy Solar Boat Team.

FIGURE 19. Under gentle weather conditions, the boat is able to sail in bays and the open sea, such as here during the Monaco Solar Boat Challenge.

FIGURE 20. TU Delft Solar Boat Team 2016 with their Solar Boat.